HHS Public Access

Author manuscript

Sci Signal. Author manuscript; available in PMC 2015 August 10.

Published in final edited form as:

Sci Signal. ; 8(363): ra15. doi:10.1126/scisignal.2005667.

Activation of TRPV1 channels inhibits mechanosensitive Piezo channel activity by depleting membrane phosphoinositides

Istvan Borbiro, **Doreen Badheka**, and **Tibor Rohacs***

Department of Pharmacology and Physiology, Rutgers, New Jersey Medical School, Newark, NJ, 07103

Abstract

Capsaicin is an activator of the heat-sensitive TRPV1 (transient receptor potential vanilloid 1) ion channels and has been used as a local analgesic. We found that activation of TRPV1 channels with capsaicin either in dorsal root ganglion neurons or in a heterologous expression system inhibited the mechanosensitive Piezo1 and Piezo2 channels by depleting phosphatidylinositol 4,5-bisphosphate [$PI(4,5)P_2$] and its precursor PI(4)P from the plasma membrane through Ca^{2+}-induced phospholipase Cδ (PLCδ) activation. Experiments with chemically inducible phosphoinositide phosphatases and receptor-induced activation of PLCβ indicated that inhibition of Piezo channels required depletion of both PI(4)P and $PI(4,5)P_2$. The mechanically activated current amplitudes decreased substantially in the excised inside-out configuration, where the membrane patch containing Piezo1 channels is removed from the cell. $PI(4,5)P_2$ and PI(4)P applied to these excised patches inhibited this decrease. Thus, we concluded that Piezo channel activity requires the presence of phosphoinositides, and the combined depletion of $PI(4,5)P_2$ or PI(4)P reduces channel activity. In addition to revealing a role for distinct membrane lipids in mechanosensitive ion channel regulation, these data suggest that inhibition of Piezo2 channels may contribute to the analgesic effect of capsaicin.

INTRODUCTION

Mechanosensation is an essential process involved in a variety of biological phenomena. Mechanically activated (MA) ion channels that are activated by membrane stretch are generally thought to mediate many aspects of mechanotransduction (1). Piezo1 and Piezo2 are nonselective Ca^{2+}-permeable cation channels that are emerging as important mediators of various aspects of mechanotransduction (2–4). Unlike previous candidates, they consistently produce large, rapidly inactivating MA currents in recombinant systems (4–10). Both channels are abundant in organs with mechanical functions, such as lungs, bladder, skin, and somatosensory dorsal root ganglion (DRG) neurons (4). Gain-of-function mutations in Piezo1 (11,12) cause hereditary xerocytosis (13), a disease associated with

*Corresponding author: tel: 973-972-4464, fax: 973-972-7950, tibor.rohacs@rutgers.edu.

Author Contributions: IB designed the experiments, performed most of the experiments, analyzed the data and wrote the paper; TR designed the experiments, directed the research and wrote the paper. DB designed and performed some experiments.

Competing interests: The authors declare no competing interests.

Data and materials availability: Plasmids are either available from T. R. upon request, or requests are referred to the scientist supplying them.

dehydrated red blood cells and mild to moderate hemolytic anemia. Gain-of-function mutations in Piezo2 cause distal arthrogryposis (14), a disease characterized by multiple distal contractures, ophthalmoplegia, and restrictive lung disease. Global genetic ablation of either *Piezo1* (15) or *Piezo2* (8) are embryonic lethal in mice. Knock down of Piezo2 using shRNA eliminates rapidly adapting MA currents in DRG neurons (4), and selective genetic knockout of *Piezo2* in the skin produces sensory deficits of the mechanosensitive Merkel cells (16,17). Combined deletion of *Piezo2* in adult DRG neurons and in Merkel cells lead to profound loss of touch sensation (18).

Phosphoinositides are important regulators of many different biological processes (19). Phosphatidylinositol 4,5-bisphosphate [$PI(4,5)P_2$] and its precursor PI(4)P are the most abundant phosphoinositides in the plasma membrane, each constituting up to 1% of the lipids therein (20). Both of these lipids are substrates for phospholipase C (PLC) enzymes, even though most PLC isoforms are enzymatically more active on $PI(4,5)P_2$ than on PI(4)P (21). $PI(4,5)P_2$ has a general role in regulating ion channels (22) and integrity of the cytoskeleton (23). $PI(4,5)P_2$ may also be involved in mechanotransduction mediated by cytoskeletal elements in hair cells (24), but its role in the regulation of the putative mechanosensitive channel has not been examined.

Transient receptor potential vanilloid 1 (TRPV1) channels are present in nociceptive DRG neurons and are activated by noxious heat and by capsaicin, a pungent compound in chili peppers. Capsaicin has long been used topically as local analgesic, but how it inhibits mechanical pain is not known (25). Deletion of the single *Piezo* gene in *Drosophila melanogaster* reduced the sensitivity of the flies to noxious mechanical stimuli (26), and knock down of the mouse *Piezo2* gene inhibited mechanical allodynia evoked by nerve ligation (27), suggesting the involvement of Piezo channels in mechanical pain. Piezo2 is present in some of TRPV1-positive mouse DRG neurons (4), and capsaicin-sensitive DRG neurons in rat mainly display rapidly adapting MA currents (28), which are likely mediated by Piezo2. Here, we performed electrophysiological experiments to test the effects of capsaicin-induced activation of TRPV1 channels on the activity of MA currents in DRG neurons and Piezo channels expressed heterologously in HEK293 cells.

We found that activation of TRPV1 by capsaicin inhibited rapidly adapting MA currents in DRG neurons. Heterologously expressed Piezo2 or Piezo1 channels were also inhibited upon activation of TRPV1 by capsaicin, and this effect required extracellular Ca^{2+}. Inclusion of $PI(4,5)P_2$ or PI(4)P in the whole-cell patch pipette alleviated the inhibitory effect of capsaicin, suggesting the involvement of the Ca^{2+}-stimulated PLCδ isoforms. In contrast, we found that $G\alpha_q$-dependent activation of PLCβ by the human muscarinic receptor 1 (hM1) only marginally inhibited Piezo1 currents. Fluorescence-based monitoring of $PI(4,5)P_2$ and PI(4)P revealed substantial differences in phosphoinositide changes induced by the two PLC-activating pathways, which may explain the differential inhibition of Piezo channels. We found that depletion of $PI(4,5)P_2$ and its precursor PI(4)P using a chemically inducible phosphatase inhibited Piezo1 currents. In excised inside-out patch experiments, Piezo1 currents persisted in a solution containing $PI(4,5)P_2$ and PI(4)P, but decreased substantially without these lipids. In conclusion, our data showed that $PI(4,5)P_2$

and PI(4)P are important cofactors for maintaining Piezo channel activity and indicated that Ca^{2+} influx through TRPV1 inhibits Piezo channels by depleting these phosphoinositides.

RESULTS

A subset of DRG neurons exhibits MA currents that are inhibited by capsaicin

A subset of TRPV1-positive DRG neurons (24%) also expresses *Piezo2* (4). To study the effects of the activation of TRPV1 channels by capsaicin on MA currents in DRG neurons, we used TRPV1 reporter mice obtained by crossing the TRPV1-cre and ROSA-STOP-EYFP mouse lines. In this reporter line neurons that had expressed *Trpv1* during development or are actively expressing *Trpv1* are labeled with yellow fluorescent protein (YFP) (29), enabling easy visual identification of TRPV1-positive neurons in DRG preparations. To enrich for cells displaying rapidly adapting MA currents consistent with the presence of Piezo channels, we visually selected neurons on the basis of morphological criteria described earlier (8). We analyzed small YFP-positive neurons (membrane capacitance under 25 pF) and found that 70.4% of them displayed MA currents with different inactivation kinetics ranging from rapid through intermediate to slow adaptation rates (Fig. 1A). Medium and large YFP-positive neurons (membrane capacitance > 25 pF) displayed mainly intermediate adapting MA currents and did not respond to capsaicin (Fig. 1B).

Among small YFP-positive DRG neurons displaying rapidly adapting MA currents, 36% also responded to 1 μM capsaicin; in these neurons capsaicin robustly inhibited MA currents (Fig. 1C–D). In cells that did not display capsaicin-induced inward currents, MA currents were not affected by capsaicin, indicating that capsaicin did not directly inhibit Piezo2 channels (Fig. 1C–D). Neither the medium and large cells that responded to mechanical stimuli, nor the small neurons with intermediate or slowly adapting MA currents displayed capsaicin-induced currents, despite their clear YFP positivity (Fig. 1A–B). These data indicated that many of the small and medium mechanosensitive DRG neurons lost *Trpv1* expression during development.

Capsaicin inhibits MA currents when Piezo and TRPV1 channels are heterologously coexpressed

Rapidly adapting MA currents in DRG neurons are mediated by Piezo2 channels (4), thus we hypothesized that capsaicin-induced TRPV1 activation inhibited Piezo2 channels. To support this hypothesis, we performed experiments in cells from a human embryonic kidney cell line (HEK293) transiently cotransfected with TRPV1 and Piezo2. Application of 1 μM capsaicin inhibited MA currents in these cells in a manner dependent on extracellular Ca^{2+} (Fig. 2A–B).

Capsaicin also inhibited MA currents in HEK293 cells cotransfected with TRPV1 and Piezo1, the homolog of Piezo2 (Fig. 3A). MA current activity did not recover after washout of capsaicin even after several minutes, when mechanical stimuli of the same intensity were applied (Fig. 3A), and larger mechanical stimuli could only elicit very small MA currents after capsaicin treatment (Fig. 3B). Capsaicin did not inhibit Piezo1 currents in cells not transfected with TRPV1 (Fig. 3C). Similar to the results with Piezo2-transfected cells (Fig.

2), the rapid inhibitory effect of capsaicin was essentially eliminated when assayed in the absence of extracellular Ca^{2+} (Fig. 3D). These data are similar to those obtained with DRG neurons and indicated a crucial role for Ca^{2+} influx through TRPV1 in mediating inhibition of MA currents. For the remainder of the heterologous expression studies, we used Piezo1 because these channels are much easier to express than Piezo2, likely due to the cellular toxicity of heterologously expressed Piezo2.

Stimuli that deplete membrane phosphoinositides inhibit Piezo1 currents

Ca^{2+} influx in response to TRPV1 activation stimulates PLCδ isoforms, leading to the depletion of $PI(4,5)P_2$ and PI(4)P both in DRG neurons (30) and in expression systems (31). To test if phosphoinositide depletion plays a role in the inhibitory effect of capsaicin, we supplemented the whole-cell patch pipette solution with $PI(4,5)P_2$ or PI(4)P and tested the effect of capsaicin on Piezo1 currents. This intracellular application of $PI(4,5)P_2$ or PI(4)P attenuated the inhibition of MA currents by capsaicin (Fig. 3E–F). Capsaicin-induced inward TRPV1 current amplitudes in cells dialyzed with $PI(4,5)P_2$ or PI(4)P were not significantly different from those in control cells (fig. S1), thus smaller Ca^{2+} influx in the presence of excess lipids cannot account for the differences in Piezo channel inhibition. Capsaicin-induced currents in the absence of Ca^{2+} were substantially larger (fig. S1).

Activation of TRPV1 with low pH (pH=5.0) also inhibited Piezo1 currents in HEK293 cells cotransfected with TRPV1 and Piezo1 (fig. S2A). Compared to the inhibition induced by capsaicin, this low pH-mediated inhibition was less complete and had the tendency to partially recover (fig. S2A). Activation of the Ca^{2+}-permeable noxious chemical sensor TRPA1 channels with mustard oil (allyl isothiocyanate, AITC) also induced a small, but statistically significant, inhibition of Piezo1 currents (fig. S2B). The inward currents induced by mustard oil were substantially smaller than those induced by low pH or capsaicin (fig. S2C), and generally the extent of Piezo1 inhibition correlated with the current amplitudes induced by these agents (fig. S2C). Neither pH=5.0 nor AITC inhibited MA currents in cells transfected with Piezo1 but not with TRPV1 or TRPA1 (fig. S2D).

Although TRPV1 activation stimulates Ca^{2+}-regulated PLCδ enzymes (30) we investigated if stimuli that activate other PLC isoforms inhibited Piezo currents. We activated PLCβ using the hM1 agonist carbachol in HEK293 cells cotransfected with Piezo1 and hM1, which is $G\alpha_q$-coupled GPCR (32). The cotransfected HEK293 cells exhibited decreased Piezo1 currents after a 5-minute application of carbachol in experiments where the pipette solution (representing the intracellular solution) contained 2 mM ATP (Fig. 4A). However, MA current amplitudes also decreased somewhat in the absence of carbachol (control) over time (Fig. 4A), and the difference between carbachol-treated and control cells was not statistically significant when normalized to the current amplitude at the start of the experiment (Fig. 4B). Comparison of the responses to increasing mechanical stimuli at the beginning and the end of the experiments in control and carbachol-treated cells showed that the stimulus-response curves were identical (Fig. 4C). We interpreted these data to indicate that activation of PLCβ by hM1 marginally inhibited Piezo1 currents when the intracellular solution contained ATP, which is required for the resynthesis of phosphoinositides (33).

To inhibit the resynthesis of phosphoinositides, we also tested the effect of carbachol in the absence of intracellular ATP. Under these conditions, carbachol slowly but robustly inhibited Piezo1 activity (Fig. 4D), producing a significant decrease in MA currents after 5 minutes when compared with the MA currents in control cells after 5 minutes (Fig. 4E). When ATP was excluded from the intracellular solution, carbachol induced a robust shift to the right (reduction in sensitivity) of the MA current to mechanical stimulus relationship and also reduced the maximal response (Fig. 4F). In contrast to carbachol, the inhibitory effect of capsaicin was essentially the same in presence or absence on intracellular ATP (Fig. 3F).

Protein kinase C (PKC) is activated downstream of PLC isoforms, therefore we tested the effect of activating PKC with the phorbol ester phorbol 12-myristate 13-acetate (PMA). In HEK293 cells transfected with Piezo1, PMA induced a slow but significant reduction in Piezo1 currents, which was attenuated by the PKC inhibitor bisindolylmaleimide (fig. S3A–C).

To provide additional evidence that the inhibition of MA currents was mediated by depletion of phosphoinositides, rather than activation of PKC, resulting from activation of PLC, we also tested the effect of depleting phosphoinositides without activating PLC. We cotransfected HEK293 cells with Piezo1 and the chemically inducible 4′,5′-phosphatase system called pseudojanin (34). Activation of pseudojanin by rapamycin depletes $PI(4,5)P_2$ and PI(4)P without releasing second messengers, such as diacylglycerol, that could activate PKC, see methods for further details. Rapamycin inhibited MA currents in HEK293 cells coexpressing Piezo1 and pseudojanin in whole cell patch clamp experiments (Fig. 5A, left). The rapamycin-induced inhibition developed over several minutes. As a control, we confirmed that MA currents were unaffected by rapamycin-induced translocation of an inactive phosphatase (Fig. 5A, right). Furthermore, MA current amplitudes were significantly different in rapamycin-treated cells expressing the inactive or active pseudojanin (Fig. 5B). In contrast, MA currents in cells transfected with a $PI(4,5)P_2$ 5-phosphatase that converts $PI(4,5)P_2$ into PI(4)P were reduced in response to rapamycin, but the inhibition was not significant when compared with the MA currents in the cells prior to rapamycin induction (Fig. 5B).

Stimuli that activate PLCβ or PLCδ produce different changes in phosphoinositides

We hypothesized that the differences in Piezo1 current inhibition were due to distinct $PI(4,5)P_2$ and PI(4)P changes induced by the activation of different PLC isoforms upon stimulation of hM1 or TRPV1. To measure dynamic changes in phosphoinositides in the plasma membrane we cotransfected HEK293 cells with hM1 or TRPV1 and with different fluorescence resonance energy transfer (FRET)-based sensors of $PI(4,5)P_2$ or PI(4)P and measured their emission ratios after hM1 or TRPV1 activation. In all cases pairs of cyan fluorescent protein (CFP)-tagged and yellow fluorescent protein (YFP)-tagged phosphoinositide binding domains were used. A decrease in FRET ratio, due to translocation of the sensors from the plasma membrane to the cytoplasm, represents a decrease in the concentration of their respective phosphoinositide target(s) in the plasma membrane (35).

The PLCδ1-PH domain sensor monitors $PI(4,5)P_2$ (35), but the PLCδ1-PH domain also binds IP_3 in vitro (36). The R322H Tubby sensor monitors $PI(4,5)P_2$ (37) and does not bind

IP_3. We used the R322H mutant (Tubby-mut) because it is more sensitive to changes in $PI(4,5)P_2$ than the wild-type probe (38). The sensor containing two copies of the PH-domain of the protein OSH2 binds to PI(4)P and $PI(4,5)P_2$ and respond to combined depletion of these two lipids with a translocation from the plasma membrane to the cytoplasm (34).

Measurements with the Tubby-mut FRET sensor indicated similar decreases in $PI(4,5)P_2$ in response to carbachol in hM1-expressing cells and to capsaicin in TRPV1-expressing cells (Fig. 6A). Experiments with (CFP)-tagged and (YFP)-tagged PLCδ1-PH domain sensors also resulted in a decrease in FRET ratio upon stimulation of cells expressing hM1 with carbachol or stimulation of cells expressing TRPV1 with capsaicin (fig. S4A).

In cells expressing the Tubby-mut $PI(4,5)P_2$ sensor, the TRPV1 antagonist capsazepine blocked the decreased FRET ratio produced in response to capsaicin (fig. S4B), and capsaicin had essentially no effect in the absence of extracellular Ca^{2+} (fig. S4C). $PI(4,5)P_2$ depletion induced by carbachol was significantly slower than that induced by capsaicin, both when detected by the Tubby-mut sensor (Fig. 6A) or by the PLCδ1-PH sensor (fig. S4A).

With the CFP-and YFP-tagged OSH2-PH domain sensors that respond to dual depletion of PI(4)P and $PI(4,5)P_2$, we assessed PI(4)P changes upon TRPV1 and hM1 activation. We reasoned that because both carbachol and capsaicin induced robust and comparable decreases in $PI(4,5)P_2$ based on the Tubby-mut and PLCδ1-PH domain sensors (Fig. 6A, fig. S4A), differences in the signals obtained with the OSH2-PH probe likely reflected differential effects on PI(4)P in response to these two agonists. Therefore, we refer to this sensor as a PI(4)P sensor, even though it responds to parallel changes in PI(4)P and $PI(4,5)P_2$.

In cells expressing the OSH2-PH domain sensor, carbachol induced a significantly smaller decrease in the FRET ratio than capsaicin, indicating less PI(4)P depletion in the membrane upon hM1 activation (Fig. 6B). Consistent with the requirement for TRPV1 activity, the capsaicin-induced decrease in the FRET ratio of the OSH2-PH domain sensor was eliminated in the presence of capsazepine (fig. S4D). When we co-transfected HEK293 cells with the OSH2-PH domain sensor and both hM1 and TRPV1, the sequential application of carbachol and capsaicin revealed that TRPV1 activation with capsaicin further depleted PI(4)P (reduced the FRET ratio) after hM1 activation with carbachol (Fig. 6C). In contrast, carbachol did not further reduce the FRET ratio of the OSH2-PH domain sensor when TRPV1 activation with capsaicin preceded hM1 activation (Fig. 6C). In cells cotransfected with the Tubby-mut sensor, hM1, and TRPV1, the decrease in FRET ratio was independent of the order of addition of carbachol and capsaicin (Fig. 6D), indicating that TRPV1 activation and hM1 activation both depleted $PI(4,5)P_2$ to a comparable extent (Fig. 6D). A slight decrease in FRET ratio occurred when capsaicin was applied after carbachol, indicating that despite the comparable FRET decrease evoked by the two agonists, capsaicin may induce a somewhat more complete $PI(4,5)P_2$ depletion than carbachol. This decrease was only significant statistically when the data were normalized to the point before the application of capsaicin (Fig. 6D, right panel). These data indicated that the hM1 receptor, which signals through G proteins to PLCβ, produced a moderate and slow decrease of PI(4)P and a larger, but still slow, depletion of $PI(4,5)P_2$; whereas TRPV1, which signals

through Ca^{2+} to PLCδ, resulted in rapid and maximal depletion of both $PI(4,5)P_2$ and PI(4)P.

The effects of phosphoinositides in cell-free excised inside-out patches

To test the direct effects of phosphoinositides on MA currents, we performed inside-out patch clamp recordings on excised membranes from Piezo1-transfected HEK293 cells. We evoked MA currents by applying negative pressure steps through the patch pipette using a high-speed pressure clamp device (39). In the cell-attached configuration, the Piezo1-mediated MA currents showed fast inactivation at negative voltages and no inactivation at positive voltages (Fig. 7A). Upon excision, MA current activity decreased (rundown) (Fig. 7B, left graph). When patches were excised into a bath solution containing $PI(4,5)P_2$ and PI(4)P, rundown was inhibited (Fig. 7B, right graph). However, the inhibition of rundown by these two phosphoinositides was only statistically significant when the responses at positive voltages were compared between the patches excised into control bath solution and those excised into phosphoinositide-containing solution (Fig. 7C). The addition of poly-Lysine, which chelates negatively charged lipids, inhibited the MA currents (Fig. 7B–C). Once the currents had rundown, we could not reactivate the MA current by adding phosphoinositides to the bath solution in most patches, even though a slow partial reactivation occurred in some cases (fig S5).

We also measured MA currents in Piezo1-expressing *Xenopus* oocytes in excised inside-out patches. The MA currents in Piezo1-injected oocytes were more than 10 times larger than the endogenous MA currents (fig. S6A). The endogenous MA currents did not show inactivation, whereas Piezo1-injected oocytes showed substantial inactivation of MA currents at negative voltages (fig. S6A). This inactivation was slower than that observed in mammalian cells, compare Figure S6A to Figure 7A. Upon excision, currents showed a variable extent of rundown in experiments in which repetitive mechanical stimuli were applied. In patches where rundown was not observed or was slow, channel activity was generally inhibited by poly-Lysine (fig. S6C). In a small number of oocytes, we succeeded in reactivating Piezo1 currents by adding $PI(4,5)P_2$ either after poly-Lysine application (fig. S6C) or spontaneous rundown (fig. S6D–E), but in many other patches these efforts were unsuccessful (fig S6F). Similar manipulations in noninjected oocytes induced negligible MA currents (fig. S6G).

DISCUSSION

We found that capsaicin quickly and almost completely inhibited rapidly adapting Piezo2-mediated MA currents in TRPV1-positive DRG neurons. Heterologously expressed Piezo2 channels were also robustly inhibited upon TRPV1 activation, showing that components required for inhibition were not specific to DRG neurons. Stimulating TRPV1 with capsaicin or low pH also inhibited heterologously expressed Piezo1 channels. Capsaicin-induced inhibition of both channels required the presence of extracellular Ca^{2+}. This inhibitory effect persisted well after the washout of capsaicin, thus a Ca^{2+}-dependent signaling cascade is more likely to explain the prolonged effect of capsaicin than direct inhibition by Ca^{2+}. Because Piezo2 channels appeared toxic to HEK293 cells, we performed

further mechanistic studies with Piezo1 channels, which are homologs of Piezo2 and have similar channel properties (5,9,10,12).

Previously, we reported that application of capsaicin to TRPV1-positive DRG neurons activated Ca^{2+}-sensitive PLCδ enzymes, which lead to depletion of the two phosphoinositides $PI(4,5)P_2$ and PI(4)P (30). Here, we found that inclusion of $PI(4,5)P_2$ or PI(4)P alleviated capsaicin-induced inhibition of Piezo currents, indicating a potential role for phosphoinositide depletion in this phenomenon.

Distinct pathways can lead to activation of different PLC isoforms, for example $G\alpha_q$-coupled receptors activate PLCβ enzymes, whereas Ca^{2+} influx induces PLCδ activation (40). In our study, application of carbachol to cells expressing hM1 and Piezo1 only induced a marginal inhibition if the intracellular pipette solution contained ATP. Exclusion of ATP from the pipette solution resulted in a much larger inhibition of Piezo1 by carbachol. ATP serves as a substrate for lipid kinases; its absence interferes with the resynthesis of phosphoinositides. Thus, without ATP the decrease in $PI(4,5)P_2$ and PI(4)P is expected to become more pronounced and irreversible. The PKC activator PMA also inhibited Piezo1, but the minimal effect of carbachol in the presence of intracellular ATP suggested that a substantial contribution by PKC to Piezo1 inhibition was unlikely. Furthermore, the absence of ATP potentiated the effect of carbachol, which is the opposite of what is expected if PKC was a major contributor, because protein kinases also require ATP.

To test whether the different kinetics and extent of inhibition by capsaicin and carbachol were due to different effects on phosphoinositides, we monitored $PI(4,5)P_2$ and PI(4)P using various FRET-based phosphoinositide sensors. We concluded that TRPV1 activation causes a fast and robust depletion of both $PI(4,5)P_2$ and PI(4)P. Muscarinic receptor activation primarily induced a comparable, yet somewhat smaller and slower decrease of $PI(4,5)P_2$ and a substantially smaller decrease in PI(4)P. These findings are consistent with the slow and incomplete inhibition of Piezo1 currents by carbachol and the fast and complete inhibition by capsaicin. Overall, our experiments with inducible phosphatases and PLC activation indicated that Piezo1 channel activity was only inhibited upon substantial reduction in both $PI(4,5)P_2$ and PI(4)P. Piezo2 channels are likely to behave similarly, because Piezo2 is not inhibited, but rather potentiated by bradykinin (8), which only induces a moderate decrease in $PI(4,5)P_2$, and does not change in PI(4)P in DRG neurons (30). Piezo channels are similar in this respect to TRPV1, which is also only inhibited when both of these phosphoinositides are greatly depleted (30,34).

Activation of TRPV1 by low pH or activation of TRPA1, another Ca^{2+}-permeable channel, by AITC also inhibited Piezo1 channels, suggesting that Ca^{2+} influx through other pathways may also modulate Piezo channel activity. Generally, the inhibitory effect correlated with TRPV1 or TRPA1 current amplitudes, but even when low pH and capsaicin produced similar current amplitudes, capsaicin induced a more complete and less reversible inhibition than low pH. A likely explanation for this is that larger proportions of currents are carried by Ca^{2+} when TRPV1 is activated by capsaicin, than by low pH (41). It is possible that Ca^{2+}-dependent factors other than phosphoinositide depletion also contribute to inhibition of

Piezo1 currents upon TRPV1 activation, because $PI(4,5)P_2$ and PI(4)P only partially and transiently alleviated the capsaicin-induced inhibition.

To test whether $PI(4,5)P_2$ and PI(4)P directly affected Piezo1 channel activity, we performed excised inside-out patch clamp experiments, perfusing the internal side of the plasma membrane patch with control solutions or phosphoinositide-containing solutions. Piezo1 currents measured in HEK293 cells rapidly decreased after excision (rundown), which is a characteristic of phosphoinositide-dependent ion channels, and reflects the loss of $PI(4,5)P_2$ and PI(4)P from the patch membrane by lipid phosphatases (22). When we excised patches into a solution containing both $PI(4,5)P_2$ and PI(4)P, rundown of Piezo1 activity was reduced. Our efforts to reactivate Piezo1 currents after rundown were generally unsuccessful in HEK293 cells. We also measured Piezo1 currents in *Xenopus* oocytes in cell-attached and excised inside-out configurations. Although the results were quite variable, we managed to reactivate Piezo1 currents in a limited number of patches. Overall, our excised patch measurements are compatible with the phosphoinositide dependence of these channels that we observed in whole-cell experiments. However, our findings also suggested that some critical cellular component is rapidly lost after excision in most experiments. We did not address here what this lost factor could be, but it is well known that an excised patch even though it is removed from the cellular environment, is still a relatively complex system containing various cellular components, including large portions of the cortical cytoskeleton (42). Our data are somewhat similar to those observed for TRPA1 channels, where ctivation by $PI(4,5)P_2$ was only observed if the lipid was applied within a short period of time after excision (43). This contrasts with most $PI(4,5)P_2$-sensitive ion channels, which are reproducibly reactivated in excised patches even several minutes after complete rundown (31,44–46), reflecting activation by direct interactions between the lipid and the channel (47–49).

Capsaicin has been used as a topical analgesic for a long time. Its effects are complex. Initially, capsaicin evokes painful burning sensation due to activation of TRPV1, followed by hypersensitivity mainly caused by neurogenic inflammation, after which it renders neurons refractory, not only to heat and capsaicin, but also to other stimuli (25). Capsaicin inhibits mechanical hyperalgesia after plantar incision (50) and after spinal nerve transection in rats (51). Our finding that capsaicin robustly and almost irreversibly inhibits Piezo2 channels may underlie or contribute to this phenomenon. We note, however, that the analgesic effects of capsaicin are long lasting and may also involve neuronal degeneration (25).

Earlier work showed that capsaicin-responsive DRG neurons mainly display rapidly adapting MA currents (28), which were later shown to be mediated by Piezo2 channels (4). We also found that capsaicin-sensitive DRG neurons that responded to mechanical stimuli, exclusively displayed rapidly adapting MA currents. We had smaller proportion of capsaicin-responsive cells displaying MA currents, however, than those reported in rat DRG neurons (28). Genetic deletion of TRPV1-positive neurons in mice had no effect on mechanosensitivity (52), whereas acute axonal silencing of TRPV1-positive fibers in rats inhibited both acute and inflammatory mechanical pain (53). This discrepancy may reflect

species differences but could also be due to the difference between acute versus chronic intervention.

In conclusion, our data show that Piezo channels require phosphoinositides for activity. Activation of TRPV1 by capsaicin inhibits rapidly adapting MA currents in DRG neurons, as well as heterologously expressed Piezo1 and Piezo2 channels through robust Ca^{2+}-induced depletion of both of these lipids, an effect that may contribute to the local analgesic effect of capsaicin. The channels likely have very high apparent affinity for phosphoinositides, because the more moderate decreases in $PI(4,5)P_2$ and PI(4)P during PLCβ activation only marginally and very slowly inhibited Piezo1 channel activity. Phosphoinositides may activate these channels indirectly, or their effects may depend on cellular factors that are easily lost in excised patches.

MATERIALS AND METHODS

Cell culture

HEK293 cells were obtained from the American Type Culture Collection and were cultured in minimal essential medium (MEM) (Life Technologies) containing of 10% (v/v) Hyclone characterized fetal bovine serum (FBS) (Thermo Scientific), 100 IU/ml penicillin and 100 μg/ml streptomycin (Life Technologies). Cells were transiently transfected using the Effectene transfection reagent (Qiagen). Then, 24 h post-transfection, cells were trypsinized and replated on poly-L-lysine-coated round coverslips; 24–48 h post-seeding, fluorescent cells were selected for electrophysiological recordings. Cultured HEK293 cells were kept in a humidity-controlled incubator with 5% CO_2 at 37°C.

DRG neurons were isolated from 6-to 12-week-old heterozygous TRPV1-reporter mice (offspring of TRPV1-$Cre^{+/+}$ (29) and R26-STOP-$EYFP^{+/+}$ (54))as described previously (55) with some modifications. All animal procedures were approved by the Institutional Animal Care and Use Committee. DRG neurons were isolated from mice of either sex, ganglia were harvested from all spinal segments after laminectomy and removal of the spinal column and maintained in ice-cold HBSS for the duration of the isolation. Isolated ganglia were cleaned from excess nerve tissue and incubated in 2 mg/ml type I collagenase (Worthington) and 5 mg/ml dispase (Sigma) in HBSS at 37°C for 27 min, followed by mechanical trituration. Digestive enzymes were then removed after centrifugation of the cells at 100 × *g* for 5 min. Cells were then resuspended and seeded onto glass coverslips coated with a mixture of poly-D-lysine (Life Technologies) and laminin (Sigma). Neurons were maintained in culture in DMEM:F12 (1:1) supplemented with 10% FBS (Thermo Scientific) NT-4 (50 ng/ml, Sigma), NGF (100 ng/ml, Sigma), 100 IU/ml penicillin and 100 μg/ml streptomycin (Life Technologies) for 16–48 h before measurements.

Oocytes were extracted from mature female *Xenopus laevis* frogs (Xenopus Express) and digested with 0.2 mg/ml collagenase (Sigma) in OR2 solution (82.5 mM NaCl, 2 mM KCl, 1 mM $MgCl_2$ and 5 mM HEPES, pH 7.4) overnight at 16–18 °C. Defolliculated oocytes were selected and maintained in OR2 solution plus 1.8 mM $CaCl_2$ and 1% penicillin/streptomycin at 16–18 °C. cRNA (20 ng) was microinjected into each oocyte using a nanoliter-injector system (World Precision Instruments). Experiments were performed 72 hours after injection.

Fluorescence measurements

For monitoring phosphoinositides we cotransfected HEK293 cells with phosphoinositide-binding domains of different proteins fused with CFP and YFP. Under basal conditions, there are sufficient amounts of phosphoinositides in the plasma membrane such that these two fluorophores are localized at the plasma membrane and undergo FRET because of their proximity due to the two-dimensional distribution in the plasma membrane. Following a decrease in the concentration of their respective lipid targets, the sensors translocate to the cytosol, and FRET decreases (35). We measured FRET ratios between CFP and YFP upon hM1, or TRPV1 activation. The following phosphoinositide sensors were used: the CFP- and YFP-tagged PLCδ1-PH domain, which is sensitive to $PI(4,5)P_2$ (35); the sensor containing two copies of the OSH2-PH domain each pair tagged with either CFP or YFP was used to monitor changes in PI(4)P (56) and the $PI(4,5)P_2$-sensitive Tubby-R322H mutant tagged with YFP (38) together with the CFP-tagged Tubby-R322H which we created by subcloning it into the pECFP-N1 vector.

FRET measurements were performed as described earlier (31). Briefly, we used a photomultiplier-based dual-emission system mounted on an IX-71 inverted microscope (Olympus), equipped with a DeltaRAM excitation light source from Photon Technology International (PTI). Excitation wavelength was 430 nm; emission was detected parallel at 480 and 535 nm using two interference filters and a dichroic mirror to separate the two emission wavelengths. Data were collected and analyzed with the Felix3.2 program (PTI). Phase contrast and fluorescent images of DRG neurons in Figure 1 were taken with an Orca Flash 4.0 camera, mounted on an Olympus IX-81 inverted microscope. Fluorescence excitation was provided by a Lambda LS light source (Sutter Instruments).

Whole-cell patch clamp

For whole-cell patch clamp, HEK293 cells were transfected with the following cDNA constructs: The mouse Piezo1 cloned into a pcDNA3.1 IRES GFP vector (4), hM1 cloned into pCMV vector, and the rat TRPV1 cloned into the pCDNA3 vector. The rapamycin-inducible $PI(4,5)P_2$ and PI(4)P phosphatase system pseudojanin (34), which contains a plasma membrane-anchored FRB fragment of the protein mTOR and another cytoplasmic fusion protein with both a $PI(4,5)P_2$ 5-phosphatase and a PI(4)P 4-phosphatase fused to FKBP12. Rapamycin induces a heterodimerization of FKBP12 and FRB, thus translocation of the phosphatases from the cytosol to plasma membrane, which results in the depletion of $PI(4,5)P_2$ converting it to PI(4)P and then to PI (34). We also used the inactive $PI(4,5)P_2$ phosphatase as a control, and the construct that has only $PI(4,5)P_2$ 5-phosphatase activity.

Whole-cell patch clamp recordings were performed at room temperature (22–24 °C) as described previously (55). Patch pipettes were pulled from thick-walled borosilicate glass capillaries (Sutter Instruments) on a P-97 pipette puller (Sutter Instruments) to a resistance of 4–6 megaohms. After formation of gigaohm-resistance seals, the whole-cell configuration was established and MA currents were measured at a holding potential of −60 mV using an Axopatch 200B amplifier (Molecular Devices). Currents were filtered at 2 kHz using the low-pass Bessel filter of the amplifier and digitized using a Digidata 1440 unit (Molecular Devices). Measurements were conducted in normal extracellular solution containing (in

mM): 137 NaCl; 5 KCl; 1 $MgCl_2$; 2 $CaCl_2$; 10 HEPES; 10 glucose pH adjusted to 7.4 with NaOH. For experiments in Ca^{2+} free solutions, $CaCl_2$ was omitted from the extracellular solution. Normal intracellular solution consisting of (in mM): 140 K^+ gluconate, 1 $MgCl_2$, 2 Na_2ATP, 5 EGTA, 10 HEPES, pH adjusted to 7.2 with KOH. Intracellular solution containing 4 mM MgATP (Fig. 3F), was also supplemented with 4 mM $MgCl_2$. For experiments with hM1 the normal intracellular solution was complemented with 0.2 mM Na_2GTP. Series resistance was not compensated for whole-cell experiments; measurements with access resistances 5–15 megaohm were used for analysis.

Mechanical stimulation of isolated DRG neuron somata and HEK293 cells in whole-cell experiments was performed using a heat-polished glass pipette (tip diameter approximately 3 μm), controlled by a piezo-electric crystal drive (Physik Instrumente), positioned at 60 degrees to the surface of the cover glass. The probe was positioned so that a 10-μm movement did not visibly contact the cell but that an 11.5-μm stimulus produced an observable membrane deflection. Steadily increasing series of mechanical steps from 12 μm in 0.4-μm increments were applied at 15 s intervals in at the beginning of most experiments. Submaximal stimuli (3.6 – 5.6 μm), based on these step protocols for each cell, were applied at 30 s intervals in time-course protocols. When cells showed significant swelling upon repetitive mechanical stimulation, measurements were discarded (57).

We classified the mechanosensitive DRG neurons into three groups on the basis of the inactivation properties of their MA currents. Cells displaying currents with rapidly and completely inactivating currents (Tau=22.9 ± 3.1 ms) during the 200 ms stimulus were referred to as RA mechanosensors, cells with slow inactivation and more than half of the peak remaining activity at the end of stimulus were called slowly adapting. Cells showing slower inactivation than RA cells (Tau=61.2 ± 6.6 ms) and with significant remaining current at the end of stimulus are called intermediately adapting (58).

Excised inside-out patch clamp

Excised inside-out patch clamp experiments on HEK293 cells were performed with borosilicate glass pipettes (World Precision Instruments) of 1.1 – 1.5 megaohm resistance. The electrode pipette contained normal extracellular solution. After establishing gigaohm resistance seals on HEK293 cells, the currents were measured using an Axopatch 200B amplifier (Molecular Devices). The holding potential was 0 mV, and mechanical stimulations were applied during steps to −60 mV and +60 mV. The perfusion solution contained 140 mM K^+ gluconate, 10 mM HEPES, 5 mM EGTA, 1 $MgCl_2$ with the pH adjusted to 7.4.

Excised inside-out macropatch experiments on *Xenopus* laevis oocytes were performed as described (59). Oocytes were injected with the cRNA of Piezo1 transcribed from Piezo1 cloned in the pGEMSH oocyte vector (59). We used borosilicate glass pipettes (World Precision Instruments, Sarasota, FL) of 0.8–1.7 megaohm resistance. The electrode pipette contained 96 mM NaCl, 2 mM KCl, 1 mM $MgCl_2$, and 5 mM HEPES (pH 7.4). After establishing gigaohm resistance seals on devitellinized *Xenopus* oocytes, currents were measured using an Axopatch 200B amplifier (Molecular Devices). In some experiments, we used a step protocol in which the holding potential was 0 mV and mechanical stimulations

were applied during steps to −80 mV and +80 mV. The perfusion solution contained 96 mM KCl, 5 mM EGTA, and 10 mM HEPES, with pH adjusted to 7.4.

Mechanical stimulation of excised inside-out patches was performed using a high-speed pressure clamp (39) (HSPC-1, ALA Scientific) controlled by pClamp 9.0 software (Molecular Devices).

Materials

Natural phosphoinositides (purified from porcine brain) mainly consisting of arachydonyl and stearyl side chains were purchased from Avanti Polar Lipids. Carbamyl-choline (carbachol), capsaicin and rapamycin were purchased from Sigma. Stock solutions (1000x concentration) for rapamycin were prepared in DMSO. Capsaicin stock was prepared in ethanol (1000x concentration or higher). Carbachol stocks were prepared in deionized water.

Data analysis

Data is presented as mean ± standard error of the mean (SEM). Homogeneity of variances was determined on all datasets using Levene's test. Groups showed equal variances, thus they were analyzed for statistically significant differences using analysis of variance (ANOVA) or one-sample Student's t-test, where applicable. Bonferroni test was applied in multiple comparisons.

Supplementary Material

Refer to Web version on PubMed Central for supplementary material.

Acknowledgments

The mouse Piezo1 cloned into a pcDNA3.1 IRES GFP vector was gift from Dr. A. Patapoutian (Scripps Research Institute), the hM1 cloned into pCMV vector was a gift from Dr. D.E. Logothetis (Virginia Commonwealth University), and the rat TRPV1 cloned into the pCDNA3 vector was a gift from Dr. D. Julius (UCSF). The plasmids for the rapamycin-inducible phosphatase system pseudojanin was a gift from Dr. G.R. Hammond (NIH). The CFP- and YFP-tagged PLCδ1-PH domain and OSH2-PH domains were provided by Dr. T. Balla (NIH), and the Tubby-R322H mutant tagged with YFP was a gift from Dr. A. Tinker, University College London. The insightful comments of the members of the Rohacs lab were highly appreciated.

Funding: This work was supported by NIH grants NS055159 and GM093290 and a grant from the New Jersey Health Foundation to T.R.

References

1. Sachs F. Stretch-activated ion channels: what are they? Physiology (Bethesda). 2010; 25:50–56. [PubMed: 20134028]
2. Delmas P, Coste B. Mechano-gated ion channels in sensory systems. Cell. 2013; 155:278–284. [PubMed: 24120130]
3. Nilius B. Pressing and squeezing with Piezos. EMBO Rep. 2010; 11:902–903. [PubMed: 21052093]
4. Coste B, Mathur J, Schmidt M, Earley TJ, Ranade S, Petrus MJ, Dubin AE, Patapoutian A. Piezo1 and Piezo2 are essential components of distinct mechanically activated cation channels. Science. 2010; 330:55–60. [PubMed: 20813920]
5. Bae C, Gottlieb PA, Sachs F. Human PIEZO1: removing inactivation. Biophys J. 2013; 105:880–886. [PubMed: 23972840]

6. Bae C, Sachs F, Gottlieb PA. The mechanosensitive ion channel Piezo1 is inhibited by the peptide GsMTx4. Biochemistry. 2011; 50:6295–6300. [PubMed: 21696149]
7. Coste B, Xiao B, Santos JS, Syeda R, Grandl J, Spencer KS, Kim SE, Schmidt M, Mathur J, Dubin AE, Montal M, Patapoutian A. Piezo proteins are pore-forming subunits of mechanically activated channels. Nature. 2012; 483:176–181. [PubMed: 22343900]
8. Dubin AE, Schmidt M, Mathur J, Petrus MJ, Xiao B, Coste B, Patapoutian A. Inflammatory signals enhance piezo2-mediated mechanosensitive currents. Cell Rep. 2012; 2:511–517. [PubMed: 22921401]
9. Gottlieb PA, Bae C, Sachs F. Gating the mechanical channel Piezo1: a comparison between whole-cell and patch recording. Channels (Austin). 2012; 6:282–289. [PubMed: 22790451]
10. Gottlieb PA, Sachs F. Piezo1: properties of a cation selective mechanical channel. Channels (Austin). 2012; 6:214–219. [PubMed: 22790400]
11. Albuisson J, Murthy SE, Bandell M, Coste B, Louis-Dit-Picard H, Mathur J, Feneant-Thibault M, Tertian G, de Jaureguiberry JP, Syfuss PY, Cahalan S, Garcon L, Toutain F, Simon Rohrlich P, Delaunay J, Picard V, Jeunemaitre X, Patapoutian A. Dehydrated hereditary stomatocytosis linked to gain-of-function mutations in mechanically activated PIEZO1 ion channels. Nat Commun. 2013; 4:1884. [PubMed: 23695678]
12. Bae C, Gnanasambandam R, Nicolai C, Sachs F, Gottlieb PA. Xerocytosis is caused by mutations that alter the kinetics of the mechanosensitive channel PIEZO1. Proc Natl Acad Sci U S A. 2013; 110:E1162–1168. [PubMed: 23487776]
13. Zarychanski R, Schulz VP, Houston BL, Maksimova Y, Houston DS, Smith B, Rinehart J, Gallagher PG. Mutations in the mechanotransduction protein PIEZO1 are associated with hereditary xerocytosis. Blood. 2012; 120:1908–1915. [PubMed: 22529292]
14. Coste B, Houge G, Murray MF, Stitziel N, Bandell M, Giovanni MA, Philippakis A, Hoischen A, Riemer G, Steen U, Steen VM, Mathur J, Cox J, Lebo M, Rehm H, Weiss ST, Wood JN, Maas RL, Sunyaev SR, Patapoutian A. Gain-of-function mutations in the mechanically activated ion channel PIEZO2 cause a subtype of Distal Arthrogryposis. Proc Natl Acad Sci U S A. 2013; 110:4667–4672. [PubMed: 23487782]
15. Ranade SS, Qiu Z, Woo SH, Hur SS, Murthy SE, Cahalan SM, Xu J, Mathur J, Bandell M, Coste B, Li YS, Chien S, Patapoutian A. Piezo1, a mechanically activated ion channel, is required for vascular development in mice. Proc Natl Acad Sci U S A. 2014
16. Maksimovic S, Nakatani M, Baba Y, Nelson AM, Marshall KL, Wellnitz SA, Firozi P, Woo SH, Ranade S, Patapoutian A, Lumpkin EA. Epidermal Merkel cells are mechanosensory cells that tune mammalian touch receptors. Nature. 2014; 509:617–621. [PubMed: 24717432]
17. Woo SH, Ranade S, Weyer AD, Dubin AE, Baba Y, Qiu Z, Petrus M, Miyamoto T, Reddy K, Lumpkin EA, Stucky CL, Patapoutian A. Piezo2 is required for Merkel-cell mechanotransduction. Nature. 2014; 509:622–626. [PubMed: 24717433]
18. Ranade SS, Woo SH, Dubin AE, Moshourab RA, Wetzel C, Petrus M, Mathur J, Begay V, Coste B, Mainquist J, Wilson AJ, Francisco AG, Reddy K, Qiu Z, Wood JN, Lewin GR, Patapoutian A. Piezo2 is the major transducer of mechanical forces for touch sensation in mice. Nature. 2014; 516:121–125. [PubMed: 25471886]
19. Balla T. Phosphoinositides: tiny lipids with giant impact on cell regulation. Physiol Rev. 2013; 93:1019–1137. [PubMed: 23899561]
20. Fruman DA, Meyers RE, Cantley LC. Phosphoinositide kinases. Annu Rev Biochem. 1998; 67:481–507. [PubMed: 9759495]
21. Rebecchi MJ, Pentyala SN. Structure, function, and control of phosphoinositide-specific phospholipase C. Physiol Rev. 2000; 80:1291–1335. [PubMed: 11015615]
22. Suh BC, Hille B. PIP2 is a necessary cofactor for ion channel function: how and why? Annu Rev Biophys. 2008; 37:175–195. [PubMed: 18573078]
23. Saarikangas J, Zhao H, Lappalainen P. Regulation of the actin cytoskeleton-plasma membrane interplay by phosphoinositides. Physiol Rev. 2010; 90:259–289. [PubMed: 20086078]
24. Hirono M, Denis CS, Richardson GP, Gillespie PG. Hair cells require phosphatidylinositol 4,5-bisphosphate for mechanical transduction and adaptation. Neuron. 2004; 44:309–320. [PubMed: 15473969]

25. Szallasi A, Blumberg PM. Vanilloid (Capsaicin) receptors and mechanisms. Pharmacol Rev. 1999; 51:159–212. [PubMed: 10353985]
26. Kim SE, Coste B, Chadha A, Cook B, Patapoutian A. The role of Drosophila Piezo in mechanical nociception. Nature. 2012; 483:209–212. [PubMed: 22343891]
27. Eijkelkamp N, Linley JE, Torres JM, Bee L, Dickenson AH, Gringhuis M, Minett MS, Hong GS, Lee E, Oh U, Ishikawa Y, Zwartkuis FJ, Cox JJ, Wood JN. A role for Piezo2 in EPAC1-dependent mechanical allodynia. Nat Commun. 2013; 4:1682. [PubMed: 23575686]
28. Drew LJ, Wood JN, Cesare P. Distinct mechanosensitive properties of capsaicin-sensitive and-insensitive sensory neurons. J Neurosci. 2002; 22:RC228 (1–5). [PubMed: 12045233]
29. Cavanaugh DJ, Chesler AT, Jackson AC, Sigal YM, Yamanaka H, Grant R, O'Donnell D, Nicoll RA, Shah NM, Julius D, Basbaum AI. Trpv1 reporter mice reveal highly restricted brain distribution and functional expression in arteriolar smooth muscle cells. J Neurosci. 2011; 31:5067–5077. [PubMed: 21451044]
30. Lukacs V, Yudin Y, Hammond GR, Sharma E, Fukami K, Rohacs T. Distinctive changes in plasma membrane phosphoinositides underlie differential regulation of TRPV1 in nociceptive neurons. Journal of Neuroscience. 2013; 33:11451–11463. [PubMed: 23843517]
31. Lukacs V, Thyagarajan B, Varnai P, Balla A, Balla T, Rohacs T. Dual regulation of TRPV1 by phosphoinositides. J Neurosci. 2007; 27:7070–7080. [PubMed: 17596456]
32. Kruse AC, Kobilka BK, Gautam D, Sexton PM, Christopoulos A, Wess J. Muscarinic acetylcholine receptors: novel opportunities for drug development. Nat Rev Drug Discov. 2014; 13:549–560. [PubMed: 24903776]
33. Suh BC, Hille B. Recovery from muscarinic modulation of M current channels requires phosphatidylinositol 4,5-bisphosphate synthesis. Neuron. 2002; 35:507–520. [PubMed: 12165472]
34. Hammond GR, Fischer MJ, Anderson KE, Holdich J, Koteci A, Balla T, Irvine RF. PI4P and PI(4,5)P_2 Are Essential But Independent Lipid Determinants of Membrane Identity. Science. 2012; 337:727–730. [PubMed: 22722250]
35. van der Wal J, Habets R, Varnai P, Balla T, Jalink K. Monitoring agonist-induced phospholipase C activation in live cells by fluorescence resonance energy transfer. J Biol Chem. 2001; 276:15337–15344. [PubMed: 11152673]
36. Xu C, Watras J, Loew LM. Kinetic analysis of receptor-activated phosphoinositide turnover. J Cell Biol. 2003; 161:779–791. [PubMed: 12771127]
37. Santagata S, Boggon TJ, Baird CL, Gomez CA, Zhao J, Shan WS, Myszka DG, Shapiro L. G-protein signaling through tubby proteins. Science. 2001; 292:2041–2050. [PubMed: 11375483]
38. Quinn KV, Behe P, Tinker A. Monitoring changes in membrane phosphatidylinositol 4,5-bisphosphate in living cells using a domain from the transcription factor tubby. J Physiol. 2008; 586:2855–2871. [PubMed: 18420701]
39. Besch SR, Suchyna T, Sachs F. High-speed pressure clamp. Pflugers Arch. 2002; 445:161–166. [PubMed: 12397401]
40. Rohacs T. Regulation of Transient Receptor Potential channels by the phospholipase C pathway. Advances in Biological Regulation. 2013; 53:341–355. [PubMed: 23916247]
41. Samways DS, Khakh BS, Egan TM. Tunable calcium current through TRPV1 receptor channels. J Biol Chem. 2008; 283:31274–31278. [PubMed: 18775990]
42. Suchyna TM, Markin VS, Sachs F. Biophysics and structure of the patch and the gigaseal. Biophys J. 2009; 97:738–747. [PubMed: 19651032]
43. Karashima Y, Prenen J, Meseguer V, Owsianik G, Voets T, Nilius B. Modulation of the transient receptor potential channel TRPA1 by phosphatidylinositol 4,5-biphosphate manipulators. Pflugers Arch. 2008; 457:77–89. [PubMed: 18461353]
44. Hilgemann DW, Ball R. Regulation of cardiac Na^+-Ca^{2+} exchange and KATP potassium channels by PIP2. Science. 1996; 273:956–959. [PubMed: 8688080]
45. Rohacs T, Lopes CM, Michailidis I, Logothetis DE. PI(4,5)P_2 regulates the activation and desensitization of TRPM8 channels through the TRP domain. Nat Neurosci. 2005; 8:626–634. [PubMed: 15852009]

46. Sui JL, Petit-Jacques J, Logothetis DE. Activation of the atrial K_{ACh} channel by the betagamma subunits of G proteins or intracellular Na^+ ions depends on the presence of phosphatidylinositol phosphates. Proc Natl Acad Sci U S A. 1998; 95:1307–1312. [PubMed: 9448327]
47. Lukacs V, Rives JM, Sun X, Zakharian E, Rohacs T. Promiscuous activation of transient receptor potential vanilloid 1 channels by negatively charged intracellular lipids, the key role of endogenous phosphoinositides in maintaining channel activity. J Biol Chem. 2013; 288:35003–35013. [PubMed: 24158445]
48. Zakharian E, Cao C, Rohacs T. Gating of transient receptor potential melastatin 8 (TRPM8) channels activated by cold and chemical agonists in planar lipid bilayers. J Neurosci. 2010; 30:12526–12534. [PubMed: 20844147]
49. Zakharian E, Cao C, Rohacs T. Intracellular ATP supports TRPV6 activity via lipid kinases and the generation of PtdIns(4,5)P_2. FASEB J. 2011; 25:3915–3928. [PubMed: 21810903]
50. Pospisilova E, Palecek J. Post-operative pain behavior in rats is reduced after single high-concentration capsaicin application. Pain. 2006; 125:233–243. [PubMed: 16797124]
51. Kim SM, Kim J, Kim E, Hwang SJ, Shin HK, Lee SE. Local application of capsaicin alleviates mechanical hyperalgesia after spinal nerve transection. Neurosci Lett. 2008; 433:199–204. [PubMed: 18242851]
52. Mishra SK, Tisel SM, Orestes P, Bhangoo SK, Hoon MA. TRPV1-lineage neurons are required for thermal sensation. EMBO J. 2011; 30:582–593. [PubMed: 21139565]
53. Brenneis C, Kistner K, Puopolo M, Segal D, Roberson D, Sisignano M, Labocha S, Ferreiros N, Strominger A, Cobos EJ, Ghasemlou N, Geisslinger G, Reeh PW, Bean BP, Woolf CJ. Phenotyping the function of TRPV1-expressing sensory neurons by targeted axonal silencing. J Neurosci. 2013; 33:315–326. [PubMed: 23283344]
54. Srinivas S, Watanabe T, Lin CS, William CM, Tanabe Y, Jessell TM, Costantini F. Cre reporter strains produced by targeted insertion of EYFP and ECFP into the ROSA26 locus. BMC Dev Biol. 2001; 1:4. [PubMed: 11299042]
55. Yudin Y, Lukacs V, Cao C, Rohacs T. Decrease in phosphatidylinositol 4,5-bisphosphate levels mediates desensitization of the cold sensor TRPM8 channels. J Physiol. 2011; 589:6007–6027. [PubMed: 22005680]
56. Balla A, Kim YJ, Varnai P, Szentpetery Z, Knight Z, Shokat KM, Balla T. Maintenance of hormone-sensitive phosphoinositide pools in the plasma membrane requires phosphatidylinositol 4-kinase IIIalpha. Mol Biol Cell. 2008; 19:711–721. [PubMed: 18077555]
57. Hamill OP, McBride DW Jr. Induced membrane hypo/hyper-mechanosensitivity: a limitation of patch-clamp recording. Annu Rev Physiol. 1997; 59:621–631. [PubMed: 9074780]
58. Rugiero F, Drew LJ, Wood JN. Kinetic properties of mechanically activated currents in spinal sensory neurons. J Physiol. 2010; 588:301–314. [PubMed: 19948656]
59. Rohacs T. Recording macroscopic currents in large patches from Xenopus oocytes. Methods Mol Biol. 2013; 998:119–131. [PubMed: 23529425]

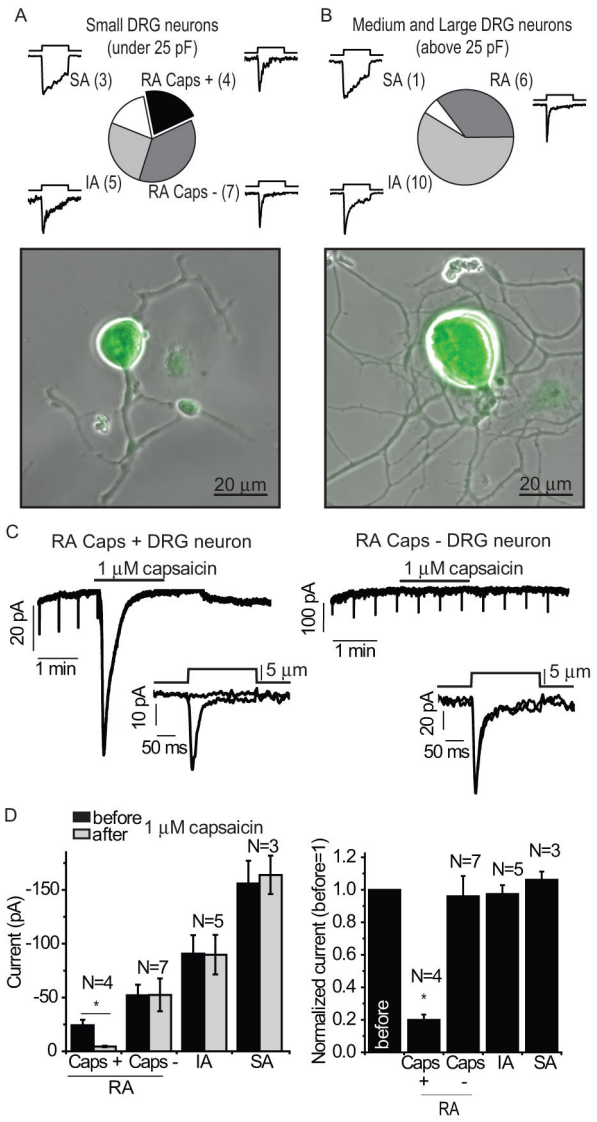

Figure 1.

The effects of capsaicin on whole-cell MA currents in DRG neurons isolated from TRPV1 reporter mice. (A) Pie chart showing the distribution of the rapidly adapting (RA), intermediate adapting (IA), and slowly adapting (SA) MA currents in small YFP-positive neurons. The RA group is subdivided into cells that respond to 1 µM capsaicin with large inward currents (Caps +) and cells that did not (Caps −). The numbers in parenthesis are the number of neurons tested in each group. None of the IA and SA cells responded to capsaicin. (B) Pie chart showing the distribution of the different types of MA currents in medium and large YFP-positive neurons. None of these neurons responded to capsaicin. Bottom panels in A and B show overlay of fluorescent and phase contrast images of a small and large neuron, respectively. (C) A representative traces recorded at −60 mV with mechanical stimulation every 30 seconds in a capsaicin-responsive neuron (left) and a nonresponsive neuron (right); the application of 1 µM capsaicin is indicated by the horizontal bars. The downward spikes correspond to the individual MA current evoked by

the repetitive mechanical stimuli. Insets show individual MA currents on enlarged time scales before and after the application of capsaicin; the mechanical step protocol, indicating the displacement of the mechanical probe is also shown. (D) Statistical analysis for small neurons showing the raw data (left) and normalized data (right) of peak MA currents measured before and after capsaicin. * $p<0.05$, Analysis of Variance (ANOVA)

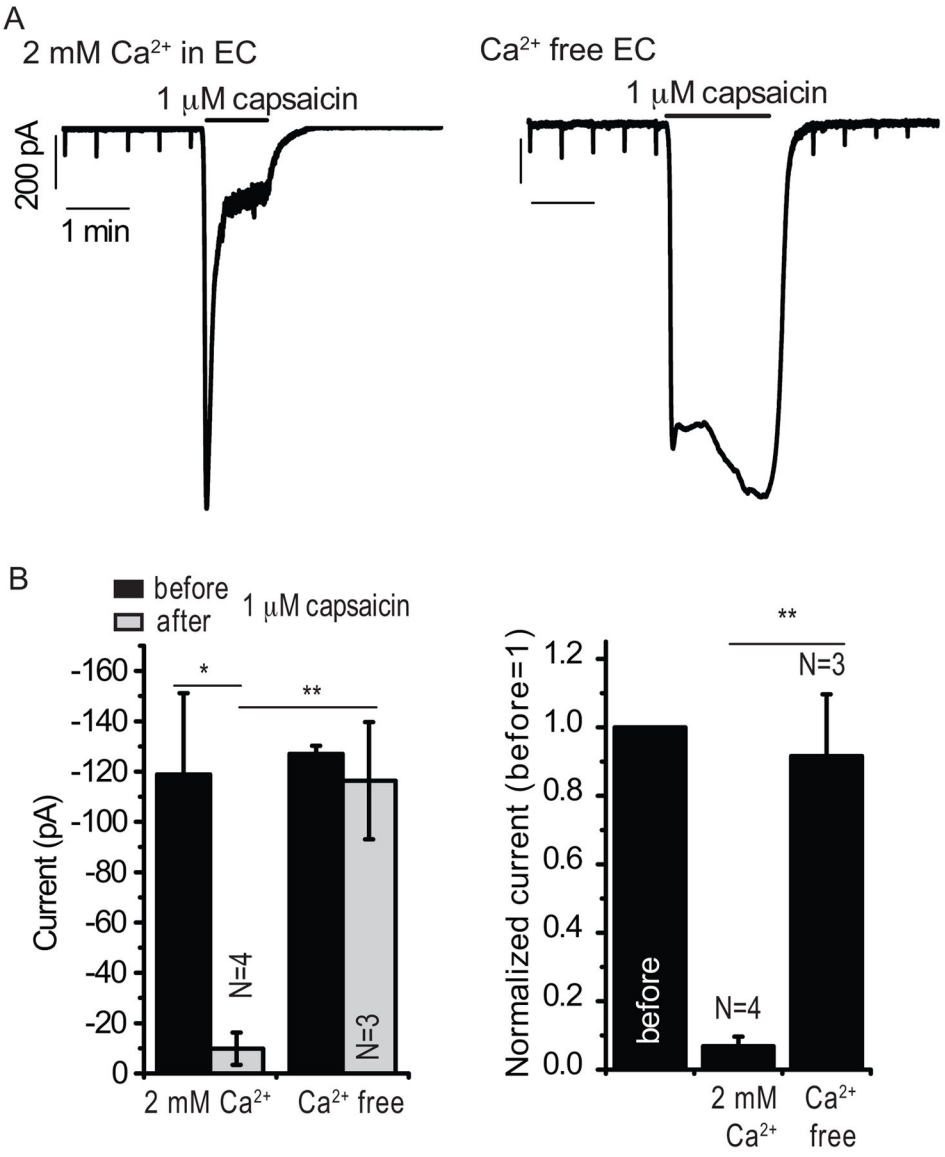

Figure 2.

The effects of TRPV1 activation on Piezo2-mediated MA currents. HEK293 cells were transiently cotransfected with Piezo2 and TRPV1, and MA currents were measured in whole-cell patch clamp experiments at −60 mV. (A) Cellular responses to repeated mechanical stimuli applied every 30 seconds recorded with application of 1 μM capsaicin in 2 mM Ca^{2+} containing (left) and Ca^{2+} free (right) extracellular (EC) solution. (B) Statistical analysis shows raw data (left) and normalized data (right) before and after the application of capsaicin. *p<0.05, **p<0.01, ANOVA

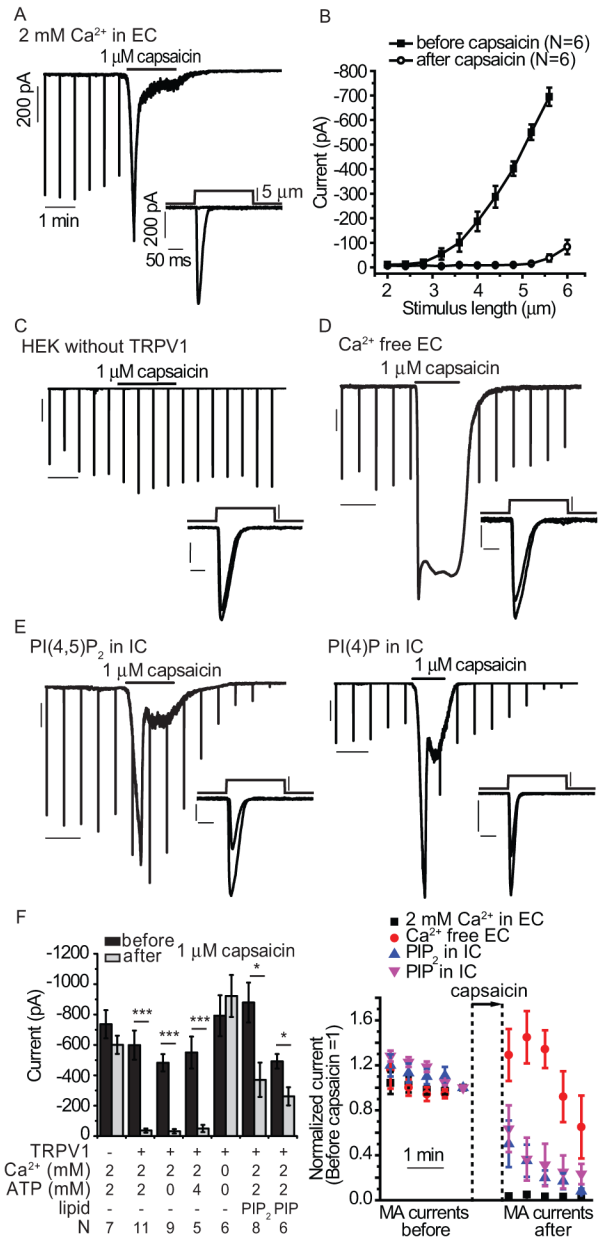

Figure 3.

The effects of TRPV1 activation on Piezo1-mediated MA currents. HEK293 cells were transiently cotransfected with Piezo1 and TRPV1, and MA currents were measured in whole-cell patch clamp experiments at −60 mV. (A) Responses to repeated mechanical stimuli applied every 30 seconds recorded with the application of 1 μM capsaicin as indicated. Insets throughout the figure show individual MA currents in response to a mechanical step of the same experiment before and after the application of capsaicin. Scale indicator lines identical to those in this panel were used throughout the figure. (B) Stimulus-response curves before and after the application of capsaicin. (C) Representative trace in a cell not transfected with TRPV1. (D) Representative trace of a Piezo1 and TRPV1 cotransfected cell assayed in the absence of extracellular Ca^{2+}. (E) Representative trace of a

Piezo1 and TRPV1 cotransfected cell assayed in normal extracellular (2 mM) Ca^{2+} with 40 μM $PI(4,5)P_2$ (left) or 40 μM PI(4)P (right) in the intracellular (IC) solution. (F) Left: statistical summary of current amplitudes before and after the application of capsaicin including those measured in the presence of the indicated concentrations of MgATP in the patch pipette. Right: the time course of the effect of $PI(4,5)P_2$ (PIP_2), PI(4)P (PIP), and Ca^{2+}-free EC solution. Data in all measurements were normalized to the current amplitudes before the application of capsaicin, individual MA current amplitudes every 30 seconds are shown (mean ± SEM). Capsaicin (1 μM) was applied for 120 sec in most measurements (range 60 – 150 s). To obtain comparable time courses, the time scale of each measurement was synchronized again to the first point after the washout of capsaicin. *$p<0.05$, ***$p<0.001$, ANOVA

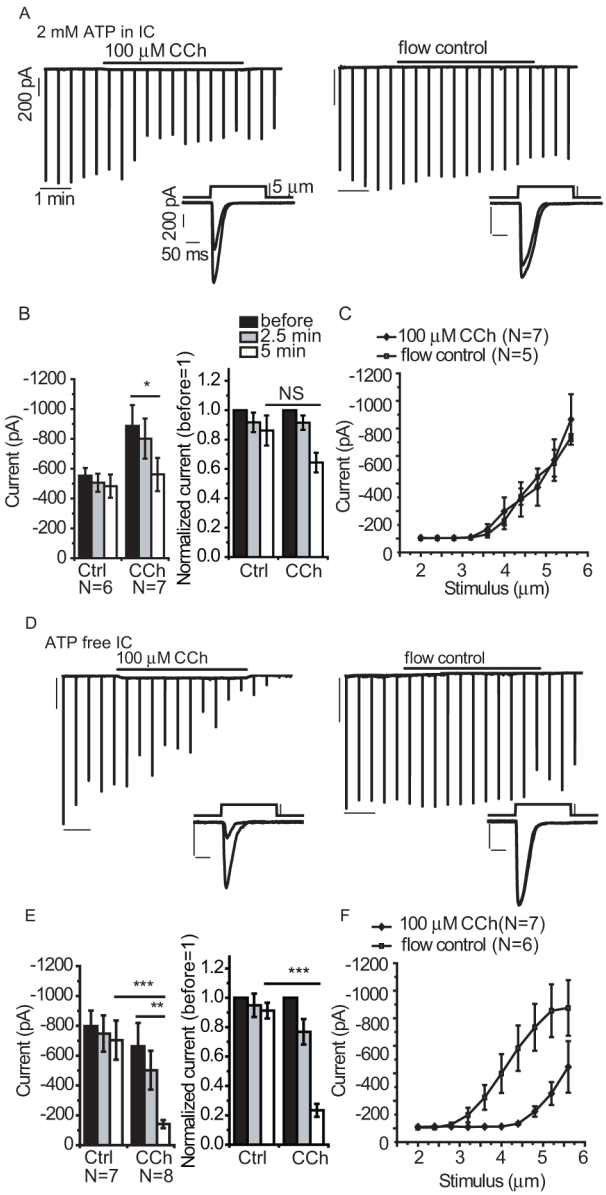

Figure 4.

The effects of hM1 activation on Piezo1-mediated MA currents. HEK293 cells were transiently cotransfected with Piezo1 and hM1 and MA currents were measured in whole-cell patch clamp experiments at −60 mV with mechanical stimuli applied every 30 seconds. (A) Representative traces for experiments with 2 mM ATP-containing IC solution in the patch pipette with 5-minute application of 100 μM carbachol (CCh) (left) and control solution (right). Insets show individual MA currents recorded before and after 5-minute carbachol application or at identical times for the control cell. Scale indicator lines identical to those in this panel were used throughout the figure. (B) Statistical analysis of carbachol-treated and control groups using raw data (left) and normalized data (right) before and after 2.5 and 5 minutes of carbachol application. (C) Stimulus response curves recorded in carbachol-treated and flow control groups with increasing steps of mechanical stimuli. (D–

F) Identical experiments and data analysis with ATP-free IC solution in the patch pipette. *p<0.05, **p<0.01, ***p<0.001, NS not significant (p=0.101), ANOVA

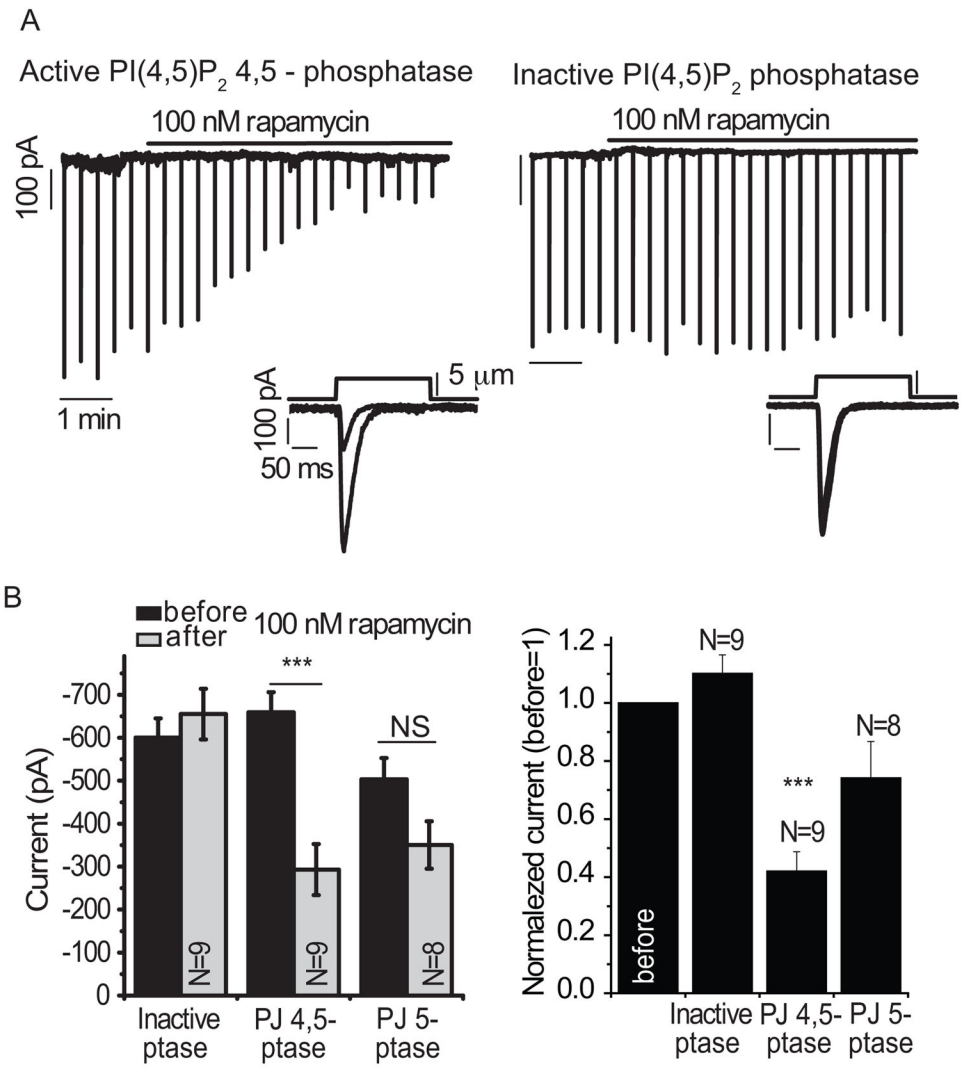

Figure 5.

The effects of rapamycin-induced plasma membrane translocation of the PI(4,5)P_2 4,5-phosphatase pseudojanin on Piezo1-mediated MA currents. HEK293 cells were cotransfected with Piezo1 and components of the pseudojanin system; MA currents were measured in whole-cell patch clamp experiments at −60 mV with mechanical stimuli applied every 30 seconds. (A) Representative traces show responses to 100 nM rapamycin during repeated mechanical stimuli in cells expressing Piezo1 and the active PI(4,5)P_2 4,5-phosphatase pseudojanin (left) or the inactive PI(4,5)P_2 phosphatase (right). Insets show individual MA current traces before and after the application of rapamycin. (B) Plots of raw data (left) and normalized data (right) show statistical analysis of peaks of MA currents in cells transfected with inactive or active PI(4,5)P_2 4,5-phosphatase (inactive ptase, PJ 4,5-ptase) or active PI(4,5)P_2 5-phosphatase (PJ 5-ptase) before and after 5 minutes of rapamycin application. ***p<0.001, NS not significant (p=0.128); ANOVA and t-test

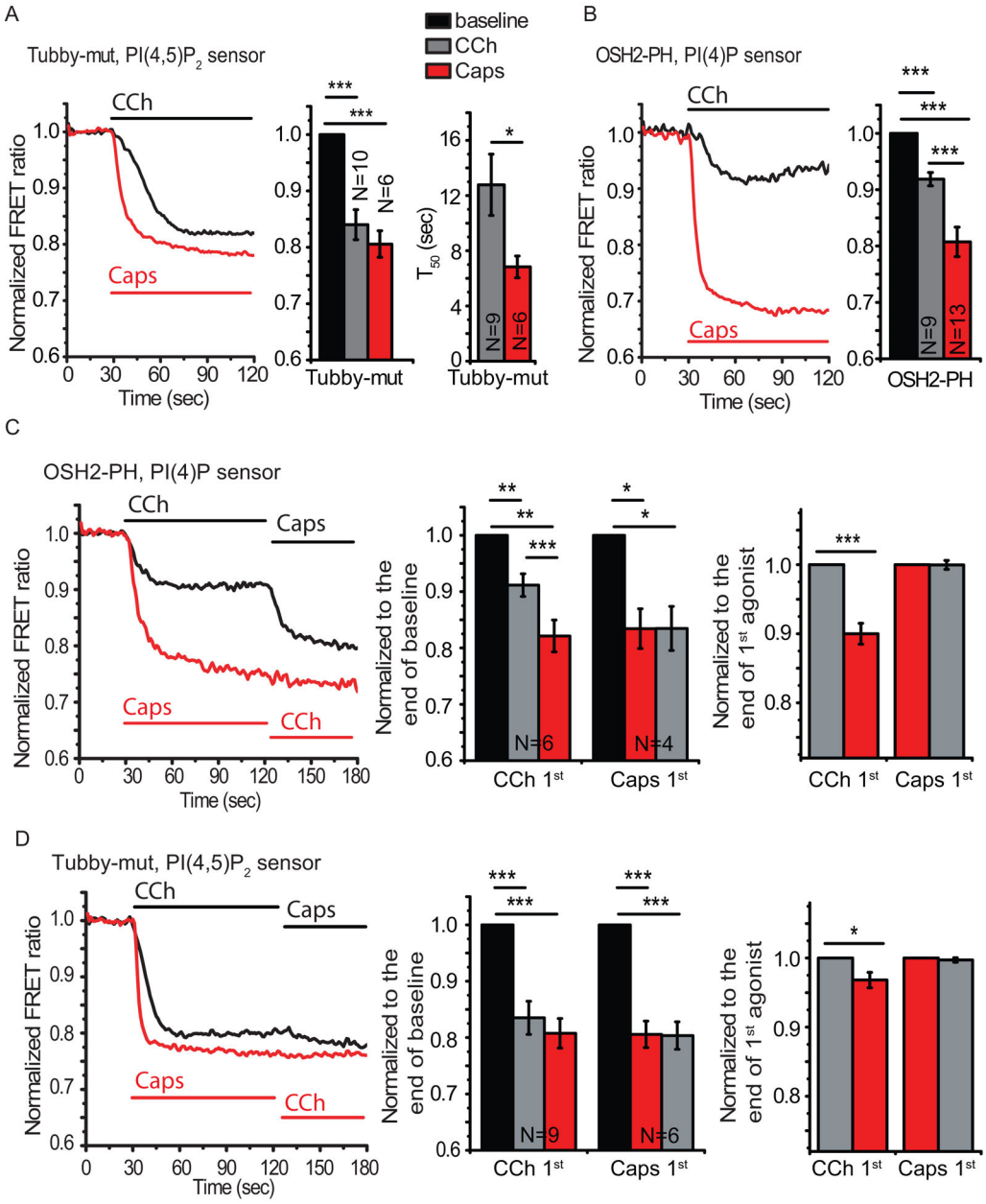

Figure 6.

Fluorescence-based PI(4,5)P_2 and PI(4)P measurements in HEK cells cotransfected with hM1 or TRPV1 and phosphoinositide sensors. (A) FRET measurements in cells expressing the Tubby-mut PI(4,5)P_2 sensor. Left panel shows individual traces in response to 100 μM carbachol (CCh) in an hM1-transfected cell and in response to 1 μM capsaicin in a TRPV1-transfected cell. Middle panel show statistical analysis of FRET ratios, right panel shows FRET decay half times for cells exposed to carbachol or capsaicin. (B) Individual FRET measurements in cells expressing the OSH2-PH domain PI(4)P sensor and either hM1 or TPRV1 (left) and statistical analysis of FRET ratios (right). (C) FRET measurements in cells cotransfected with the OSH2-PH sensor and both TRPV1 and hM1. The sequential

applications of 1 μM capsaicin and 100 μM carbachol are indicated by the horizontal lines in the representative traces (left). Statistical analyses of OSH2-PH FRET ratios normalized to the baseline (middle) or to the end of first agonist application (right) are shown. (D) FRET measurements in cells cotransfected with the Tubby-mut $PI(4,5)P_2$ sensor and both TRPV1 and hM1. Data are presented as in panel C. *$p<0.05$, **$p<0.01$, ***$p<0.001$, ANOVA, t-test

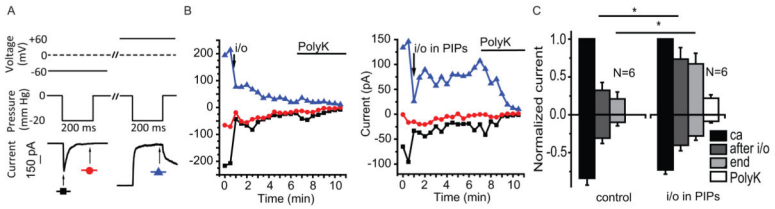

Figure 7.

The effects of PI(4,5)P_2 and PI(4)P on Piezo1-mediated MA currents in excised inside-out patches in HEK293 cells transfected with Piezo1. (A) Voltage (upper) and pressure (middle) protocols and representative MA currents (lower). The holding potential was 0 mV, a 3s long voltage step to −60 mV was applied, during which a 200 ms long negative pressure pulse was used to elicit MA currents; 15 s later a second 3 s voltage step to +60 mV was applied during which the MA currents were induced with a −20 mmHg pressure step. The protocol was repeated every 30 s. (A, lower) Individual traces with marks showing peak currents (black square) and the currents at the end of the pressure step (red circle) at −60 mV, and peak currents (blue triangle) at +60 mV, which were plotted in panel B. (B) Representative MA peaks and end currents (as marked in the lower part of A) measured when patches were excised (i/o) into control bath solution (left), or a bath solution containing 10 μM PI(4,5)P_2 and 10 μM PI(4)P (PIPs) (right). At the time periods indicated by the horizontal lines the patch was perfused with 30 μg/ml Poly-lysine (Poly K). (C) Statistical summary of peak MA currents recorded at −60 mV (downward bars) and +60 mV (upward bars) in the cell attached configuration (ca), after excision (i/o), 5 minutes after excision (end), and after application of 30 μg/ml Poly-lysine (PolyK). All data were normalized to the cell-attached current values at +60 mV *$p<0.05$, ANOVA